

Doubly-Irregular Repeat-Accumulate Codes over Integer Rings for Multi-user Communications

Fangtao Yu, Tao Yang, *Member, IEEE* and Qiuzhuo Chen

Abstract

Structured codes based on lattices were shown to provide enlarged capacity for multi-user communication networks. In this paper, we study capacity-approaching irregular repeat accumulate (IRA) codes over integer rings \mathbb{Z}_{2^m} for 2^m -PAM signaling, $m = 1, 2, \dots$. Such codes feature the property that the integer sum of K codewords belongs to the extended codebook (or lattice) w.r.t. the base code. With it, *structured binning* can be utilized and the gains promised in lattice based network information theory can be materialized in practice. In designing IRA ring codes, we first analyze the effect of zero-divisors of integer ring on the iterative belief-propagation (BP) decoding, and show the invalidity of symmetric Gaussian approximation. Then we propose a doubly IRA (D-IRA) ring code structure, consisting of *irregular multiplier distribution* and *irregular node-degree distribution*, that can restore the symmetry and optimize the BP decoding threshold. For point-to-point AWGN channel with 2^m -PAM inputs, D-IRA ring codes perform as low as 0.29 dB to the capacity limits, outperforming existing bit-interleaved coded-modulation (BICM) and IRA modulation codes over $\text{GF}(2^m)$. We then proceed to design D-IRA ring codes for two important multi-user communication setups, namely compute-forward (CF) and dirty paper coding (DPC), with 2^m -PAM signaling. With it, a physical-layer network coding scheme yields a gap to the CF limit by 0.24 dB, and a simple linear DPC scheme exhibits a gap to the capacity by 0.91 dB.

Index Terms

Coded modulation, lattice codes, physical-layer network coding, compute-forward, network information theory, multiple-access, broadcast channel, dirty paper coding

I. INTRODUCTION

The noisy channel coding theorem reveals the fundamental limits of reliable communications, and various coding techniques are developed for approaching the limits. Existing turbo, polar and low-density parity-check (LDPC) codes can yield near-capacity performance for long block lengths. Repeat-Accumulate (RA) codes proposed by Divsalar and Jin enjoy both advantages of linear encoding complexity of turbo codes and parallel decoding of LDPC codes. Irregular repeat accumulate (IRA) codes feature non-uniform

variable and check nodes degrees which give rise to improved decoding threshold [1], [2]. Using density evolution (DE) or extrinsic information transfer (EXIT) chart based optimization, well-designed IRA codes perform only a small fraction of dB away from the capacity limits of binary-input channels [3], [4].

For higher order modulation, e.g., 2^m -PAM or 2^{2m} -QAM, $m = 1, 2, \dots$, bit-interleaved coded modulation (BICM), trellis-coded modulation (TCM) and superposition-coded modulation (SCM) have been studied [5]–[7]. These conventional schemes are referred to as “*binary coding oriented*”: an off-the-shelf binary channel code is determined in the first place, and then a *many-to-one* mapping is utilized to match 2^m binary coded digits to a PAM symbol. To approach the capacity limit, these schemes require an outer-loop receiver iteration [8] that exchanges soft information between the soft-input soft-output demodulator and a bank of channel-code decoders. As each decoder may involve an inner-loop iteration by itself, the total number of decoding iterations amounts to the product of the numbers of inner-loop and out-loop iterations. Most existing practical systems incline to avoid the outer-loop iteration to reduce the implementation cost and latency, but at the expense of a significant gap to the ultimate performance.

Different from the coding-oriented schemes, Chiu proposed q -ary IRA modulation codes for q -PAM inputs [9]. This scheme is referred to as “*modulation-oriented*”: q -PAM signaling is determined in the first place, and an IRA code over $\text{GF}(q)$ is adopted whose output q -ary coded digits are *one-to-one* mapped to q -PAM symbols. Thanks to the one-to-one mapping, the outer-loop iteration is avoided while achieving the near-capacity performance. Moreover, for prime q , IRA modulation codes are lattice codes without a one-dimension shaping code, whose advance in the two-way relay channel setup was reported in [10].

A. Motivations and Necessity of Ring Codes in Multi-user Networks

For a variety of multi-user configurations, structured codes based on lattices have been exploited in solving network information theory problems [11], such as Slepian-Wolf and Wyner-Ziv problems (source coding with side information (SI) at receiver), dirty paper coding (DPC) problem (channel coding with SI at transmitter) [12], [13], physical-layer network coding (PNC) or compute-and-forward (CF) [14], interference alignment, multiple-access (MA), precoding for broadcast channel, and etc.. Using lattices codes, compelling theoretical advances by exploiting “*structured binning*” over conventional random coding have been reported, where the key notion is to efficiently compute the *bin-indices* [15]–[17]. The proofs of these results were based on the existence of “Roger-good” and “Ploeyrev-good” lattice chains [13], but no clues are given on the code construction for practical implementation.

To materialize the gains of structured binning in a practical multi-user wireless network with widely used $q = 2^m$ level PAM (or 2^{2m} -QAM) signaling, codes over integer rings \mathbb{Z}_{2^m} become particularly relevant.

To see this, first note that conventional BICM, TCM and SCM schemes are not lattice codes. Due to the many-to-one signal mapping, structured binning does not apply therein. Second, the aforementioned IRA modulation codes belong to lattice codes only for prime q . Yet, for non-prime $q = 2^m$, the IRA modulation codes operate over the extended Galois field $\text{GF}(2^m)$ [9]. The additive and multiplication rules of $\text{GF}(2^m)$ are not identical to the integer operations of \mathbb{Z}_{2^m} , hence structured binning does not apply, either. This motivates us to study ring codes over integers \mathbb{Z}_{2^m} .

B. Main Contributions

To the best of our knowledge, the design of capacity-approaching ring codes with 2^m -PAM signaling remains open. In this paper, we first analyze the effect of zero-divisor elements in \mathbb{Z}_{2^m} on the belief-propagation (BP) decoding. We show the invalidity of the symmetric Gaussian approximation (with which the results in [9] are built) in the statistics of the soft information exchanged in the component decoders. Then, we propose a new doubly IRA (D-IRA) ring code, featuring *irregular multiplier distribution* and *irregular node-degree distribution*, that can restore the symmetry and optimize the decoding threshold. The degree profile optimization based on extrinsic information transfer chart (EXIT) curve-fitting is conducted [18]. We demonstrate that our proposed D-IRA ring codes perform as low as 0.29 dB away from the AWGN capacity limits with 2^m -PAM inputs, and outperform other baseline code-modulation schemes.

We then move on to the design of D-IRA ring codes for the CF and DPC settings operated with structured binning [14], [19]–[21], with 2^m -PAM signaling. With it, it is shown that the D-IRA ring-coded PNC yields a gap to the CF capacity limit by 0.24 dB, and a simple linear DPC scheme exhibits a gap to the interference-free capacity by as low as 0.91 dB. D-IRA ring codes may serve as a bridging between the lattice-based network information theory and practical wireless systems.

This paper focuses on designing ring codes of 2^m -PAM signaling that achieve the near-capacity performance of some multi-user communication setups, hence the decoding thresholds (waterfall region) with long codes are primarily concerned. The code profiles optimized for long codes are also competitive choices for medium-length codes. The design of short codes require distance spectrum and weight analysis over a q -ary ring. This is out of the scope of the current paper and will be considered as a future work.

II. PRELIMINARIES OF 2^m -ARY CODES OVER INTEGER RINGS

Throughout this paper we present the real-valued model with 2^m -PAM. The complex-valued model with 2^{2m} -QAM can be easily represented by a real-valued model of doubled dimension as treated in [14] [10].

A. Ring Codes for 2^m -PAM Signaling

Let $\mathbf{w} = [w_1, \dots, w_k]^T$ denote a 2^m -ary message sequence of length k ¹. Each entry of \mathbf{w} belongs to an integer ring $\mathbb{Z}_{2^m} \triangleq \{0, 1, \dots, 2^m - 1\}$. A 2^m -ary ring code with generator matrix \mathbf{G} is employed to encode \mathbf{w} , given by

$$\mathbf{c} = \mathbf{G} \otimes \mathbf{w} \quad (1)$$

where “ \otimes ” represents matrix multiplication modulo- 2^m . The generator matrix \mathbf{G} is of size n -by- k with entries in \mathbb{Z}_{2^m} . Let \mathcal{C}^n denote the codebook which collects all valid codewords of \mathbf{c} generated by (1).

A random vector $\boldsymbol{\theta} \in \mathbb{Z}_q^n$ is generated and added on \mathbf{c} , resulting in $\mathbf{c}' = \mathbf{c} \oplus \boldsymbol{\theta}$ where “ \oplus ” represents the matrix addition modulo- 2^m . This is for the purpose of random permutation [9]. Then, each entry of \mathbf{c}' is *one-to-one* mapped to a symbol that belongs to a constellation of 2^m points. For 2^m -PAM constellation with uniformly spaced points, the mapping function $\delta(\cdot)$ is simply

$$\mathbf{x} = \delta(\mathbf{c}') = \frac{1}{\gamma} \left(\mathbf{c}' - \frac{2^m - 1}{2} \right) \in \frac{1}{\gamma} \left\{ \frac{1 - 2^m}{2}, \dots, \frac{2^m - 1}{2} \right\}^n, \quad (2)$$

implemented symbol-wisely. Here γ is a normalization factor to ensure unit average symbol energy. The information rate is $R = \frac{k}{n} \log_2 q = \frac{km}{n}$ bits/symbol.

Roughly speaking, the problem is to find a “good” structure of \mathbf{G} that achieves near-capacity, while the encoding, decoding and code optimization can be implemented with a reasonable cost.

Remark 1: The ring coded 2^m -PAM scheme differs from conventional coding-oriented schemes, where binary coded sequence \mathbf{c} is de-multiplexed into m streams $\mathbf{c}^{(1)}, \dots, \mathbf{c}^{(m)}$. Then, a *many-to-one* mapping is employed, e.g. the Grey mapping used in BICM. Such a many-to-one mapping incurs uncertainty that has to be addressed in the first place at the receiver.

Property 1: For any K codewords $\mathbf{c}_1, \mathbf{c}_2, \dots, \mathbf{c}_K \in \mathcal{C}^n$, the ring coded 2^m -PAM scheme satisfies

$$\text{mod} \left(\sum_{i=1}^K \alpha_i \mathbf{c}_i, 2^m \right) \in \mathcal{C}^n \quad (3)$$

for any integer coefficients $[\alpha_1, \dots, \alpha_K]$. In other words, the integer-sum of K codewords modulo- 2^m remains as a valid codeword, hence the name “*integer additive property*”.

This property has been intensively studied in the area of lattice codes for solving network information theory problems [12], [14], [22]. The details will be retained until Section V. This property does not hold in conventional binary coded-oriented schemes.

¹The conversion from a binary message sequence to a 2^m -ary message sequence is straightforward.

B. Rings Versus Galois Fields

Most existing works on lattice codes, low density lattice codes, and IRA modulation codes focused on prime q [23] [9], where $\text{GF}(q)$ and \mathbb{Z}_q are equivalent. The integer additive property holds therein. In practical systems utilizing BPSK to 4096-QAM signaling, non-prime $q = 2^m$ is required. The operation rules of \mathbb{Z}_{2^m} are different to those of $\text{GF}(2^m)$, and integer additive property does not hold for $\text{GF}(2^m)$ based codes. To see this, recall that $\text{GF}(2^m)$ is an extension field of $\text{GF}(2)$, which has elements $\{0, 1, \beta, \beta^2, \dots, \beta^{2^m-2}\}$ [24]. The additive rule w.r.t. these elements is determined based on the primitive element of the polynomials, which is different from that of \mathbb{Z}_{2^m} . Therefore, to enable the integer additive property for 2^m -PAM signaling, utilization of ring codes over \mathbb{Z}_{2^m} could be a must.

The ring coded 2^m -PAM is a simplified yet powerful version of nested lattice codes whilst the $\text{GF}(2^m)$ based codes are not. The fine lattice is given by the *extended codebook* w.r.t. $\mathbf{c} = \mathbf{G} \otimes \mathbf{w}$. This is also referred to as ‘‘Construction A’’ of lattice codes [14], [22]. The shaping lattice is given by $2^m\mathbb{Z}^n$, i.e., a one-dimension modulo- 2^m operation, which yields 2^m -PAM signaling. Note that this paper devotes no efforts to attain a Gaussian input distribution, although this can be interesting additive future works. Comparing to Gaussian signaling, 2^m -PAM enjoys lower implementation cost and lower peak-to-average power ratio (PAPR) that favours practical implementation.

III. PROPOSED DOUBLY-IRREGULAR REPEAT ACCUMULATE RING CODES

A. Zero-divisors in Integer Rings

Recall the integer ring $\mathbb{Z}_{2^m} = \{0, 1, \dots, 2^m - 1\}$ where the addition and multiplication are defined as

$$\begin{aligned} a \oplus b &\triangleq (a + b) \bmod 2^m, \\ a \otimes b &\triangleq (a \cdot b) \bmod 2^m. \end{aligned} \tag{4}$$

For a non-zero element $a \in \mathbb{Z}_{2^m}$, its inverse is said to exist if there is a unique element $b \in \mathbb{Z}_{2^m}$ that satisfies $a \otimes b = 1$. This unique inverse is written as a^{-1} . Not all but some of the non-zero elements have unique inverses. For a non-zero element $a \in \mathbb{Z}_{2^m}$, its *zero-multiplier* is defined as

$$M_0(a) \triangleq \min_{j>0, a \otimes j=0} j. \tag{5}$$

For the elements with unique inverses, $M_0(a) = q$. Such elements are called *regular elements*. For the elements that do not have unique inverses, $M_0(a) < q$. Such elements are called *zero-divisors*. An example of \mathbb{Z}_8 is shown in TABLE I, where $\{1, 3, 5, 7\}$ are regular elements while $\{2, 4, 6\}$ are zero-divisors.

TABLE I
EXAMPLE OF ZERO-DIVISORS WITH $q=8$.

a	1	2	3	4	5	6	7
$M_0(a)$	8	4	8	2	8	4	8

B. Repeat Accumulate (RA) Ring Code Structure

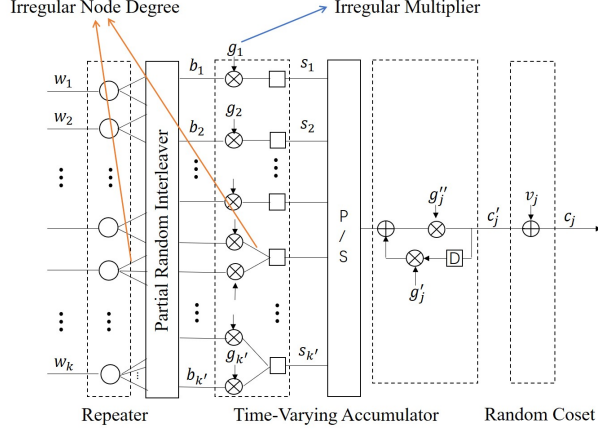


Fig. 1. Block diagram of a D-IRA code encoder. The multipliers \mathbf{g}' and \mathbf{g}'' of the time-varying accumulator are randomly selected from the regular element set with equal probability.

The block diagram of the encoder is depicted in Fig. 1. Each entry of the message sequence \mathbf{w} is referred to as an information node. The entries are repeated according to a certain degree distribution, which yields length- k' sequence $\mathbf{b}' \in \{0, \dots, 2^m - 1\}^{k'}$, $k' > k$. This sequence is interleaved, yielding $\mathbf{b} = \pi(\mathbf{b}')$. The interleaved sequence is forwarded to a bank of check-nodes (CNs). Each input edge of the CNs is associated with a multiplier with value taken in $\{1, \dots, 2^m - 1\}$. Note that the multipliers can be either regular elements or zero-divisors. The outputs of the CNs are forwarded to a time-varying accumulator, which yields the length- n codeword sequence \mathbf{c} [9]. Next \mathbf{c} is one-to-one mapped to \mathbf{x} as given in (2). For the clarity of presentation, we omit the random permutation θ .

For AWGN channel, upon receiving \mathbf{y} , the noisy observation of \mathbf{x} , the receiver first calculates the channel-intrinsic symbol-wise a posteriori probabilities (APPs). Let $c[t]$, $y[t]$, $t = 1, \dots, n$, denote the t -th entry of \mathbf{c} and \mathbf{y} , respectively. The channel-intrinsic APP for $c[t] = i$, $i = 0, \dots, 2^m - 1$, is

$$p_i^{CH}[t] \triangleq p(c[t] = i | y[t]) \propto p(y[t] | c[t] = i) = \frac{1}{\eta} \exp\left(-\frac{(y[t] - \delta(i))^2}{2\sigma_z^2}\right) \quad (6)$$

where the conversion from APP to likelihood function follows from the Bayes rule as $c[t]$ is uniformly distributed, and η is just a normalization factor to ensure $\sum_i p_i^{CH}[t] = 1$. The 2^m -level probabilities are collected by a probability vector $\mathbf{p}^{CH}[t] = [p_0^{CH}[t], \dots, p_{2^m-1}^{CH}[t]]^T$.

The APP vectors $\mathbf{p}^{CH}[t]$, $t = 1, \dots, n$, are forwarded to the iterative belief propagation (BP) decoder,

which is to yield the decision on the message sequence w . The Tanner graph of a D-IRA ring code is shown in Fig. 2. There are two types of message-propagation in BP algorithm: the messages propagated from variable nodes (VNs) to check nodes (CNs) and the messages propagated from CNs to VNs. In a generic RA structure, VNs involve 1) information nodes at the left-hand side of the interleaver and 2) parity nodes at the right-hand side of the interleaver which are attached to the channel intrinsic APPs. All nodes operate with the length- $(2^m - 1)$ probability vectors.

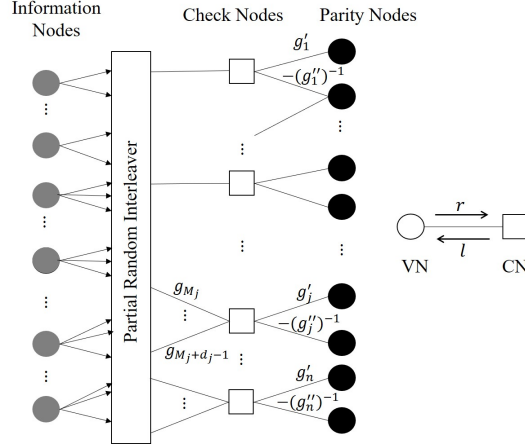


Fig. 2. Tanner graph of D-IRA.

The output probability vector of a VN of degree d_v is computed as

$$r_i = \frac{p_i \prod_{\tau=1}^{d_v-1} l_i^\tau}{\sum_{j=0}^{2^m-1} \left(p_j \prod_{\tau=1}^{d_v-1} l_j^\tau \right)}, \quad i = 0, \dots, 2^m - 1 \quad (7)$$

where l_i^τ denotes the probability of i obtained from the τ -th input edge to VN. Here, $p_i = \frac{1}{2^m}$ for information nodes and $p_i = p_i^{CH}[t]$ for parity nodes. Here we omitted the node index in the presentation.

The outputs of a CN of degree d_c are computed as

$$l_i = \sum_{a_1, \dots, a_{d-1} \in \Phi} \prod_{\tau=1}^{d-1} r_{a_\tau}^\tau \quad (8)$$

with

$$\Phi : a_1, \dots, a_{d-1} \in \mathbb{Z}_{2^m}, \bigoplus_{\tau=1}^{d-1} h_\tau a_\tau \oplus h_0 i = 0, \quad (9)$$

denoting the check-rule. Here $d = d_c + 2$ where the extra two edges are from the accumulator as in Fig. 2; $\{a_1, \dots, a_{d-1}\}$ denotes a *candidate symbol-combination* in $\{0, \dots, q-1\}^{d-1}$, referred to as a candidate, satisfying the check-rule constraint; $r_{a_\tau}^\tau$ denotes the probability of a_n obtained from the τ -th input edge, h_τ is the multiplier of the τ -th edge and h_0 is that of the output edge.

In each iteration, the above calculations are carried out and the messages are exchanged among the

VNs and CNs. The iteration stops when the hard decision of the output sequence meets the constraints of code parity-check matrix or the maximum number of iterations is reached.

C. Issues with Regular Multiplier Distribution

Definition 1: If the multipliers w.r.t. the k' edges, denoted by $\mathbf{g} = [g_1, \dots, g_{k'}]^T$, are uniformly distributed in $\{1, \dots, 2^m - 1\}$, i.e.

$$p(g = j) = \frac{1}{2^m - 1}, j = 1, \dots, 2^m - 1, \quad (10)$$

we say that the code has a *regular multiplier distribution*. On the other hand, if the multipliers are not uniformly distributed, i.e. (10) does not hold, the code is said to have an *irregular multiplier distribution*.

As seen from the code structure, each edge of CNs is associated with a multiplier g taking values $\{1, \dots, q - 1\}$. For the 2^m -ary ring codes under consideration, there are zero-divisors who have no unique inverse in $\{1, \dots, q - 1\}$, causing ambiguity in the message passing. We next illustrate the impact caused by this ambiguity issue, and presents how the proposed irregular multiplier distribution addresses it.

1) *Effect of zero-divisors on the Calculation at the Check Nodes:* Consider a CN of degree d_c . There are totally $d = d_c + 1$ input edges and one output edge in the calculation. Recall that the multipliers w.r.t the input edges are given by $[h_1, \dots, h_d]$ and that w.r.t. the output edge is given by h_0 , respectively. Let us temporarily consider that only the τ' -th input edge has a multiplier $h_{\tau'}$ which is a zero-divisor, while the multiplier of the output edge h_0 is a regular element. For given $[a_1, \dots, a_{\tau'-1}, a_{\tau'+1}, \dots, a_d]$ and i , there are multiple values of $a_{\tau'}$ that satisfy the check-rule

$$h_{\tau'} a_{\tau'} \oplus \bigoplus_{\tau=1, \tau \neq \tau'}^{d-1} h_{\tau} a_{\tau} \oplus h_0 i = 0. \quad (11)$$

This ambiguity leads to a larger number of valid candidates which are involved in the calculation of (8). If there are more than one input edges whose multipliers are zero-divisors, the impact of the ambiguity becomes more significant, and a even larger number of valid candidates are involved in the calculation of (8). This results in an effect of loosen constraint of CNs.

Next, consider that only the output edge has a multiplier h_0 of a zero-divisor, while all input edges have multipliers with regular elements. For given $[a_1, \dots, a_d]$, there are multiple values of i that satisfy the check-rule (11). The output probabilities w.r.t. these values have to be set to be identical. This increases the uncertainty in the output probability vector and reduces mutual information. If both an input edge and the output edge have zero-divisor multipliers, the ambiguity becomes even more difficult to track.

2) *Asymmetry in the LLR Vector*: For any edge, let the associated probabilities be denoted by a vector $\mathbf{p} = [p_0, \dots, p_{2^m-1}]^T$. The log-likelihood ratios (LLRs) associated with the elements in \mathbf{p} are defined as

$$\lambda_i = \log(p_0/p_i), i = 1, \dots, 2^m - 1. \quad (12)$$

We refer to $\boldsymbol{\lambda} = [\lambda_1, \dots, \lambda_{2^m-1}]^T$ as a LLR vector.

Let $\boldsymbol{\Lambda}$ collect the LLR vectors of all edges. The input LLR matrix to the check node decoder (CND), denoted by $\boldsymbol{\Lambda}_{CND,in}$, is assumed to be jointly consistent Gaussian distributed [25], [26] with parameter σ^2 . (This assumption is supported via extensive simulations.) That is, their mean and cross-covariance are $\sigma^2/2$ and auto-correlation are σ^2 . The output LLR vector is denoted by $\boldsymbol{\Lambda}_{CND,out}$ obtained via (8).

For $\text{GF}(q)$ codes with prime q , the output LLR vector is symmetric in the statistics. All the LLR elements follow the same Gaussian p.d.f., at both the VND and CND. For 2^m -ary ring codes, things start to change. Consider $m = 2$. For RA ring codes with regular multiplier distribution, i.e., the multipliers in \mathbf{g} are i.i.d. over $\mathbb{Z}_{2^m} \setminus \{0\}$, the p.d.f. for the LLR vectors are shown in Fig. 3. For the output edges with multipliers of value 2, which is a zero-divisor, the CND output probability is subject to $p_0 = p_2$, which results in a zero LLR value $\lambda_2 = 0$. Thus, the p.d.f. corresponding to λ_2 at the CND output has an impulse at value of zero. The height of the impulse is given by the ratio between the number of edges with multiplier 2 and the number of all edges. For the case with regular multiplier distribution, it is equal to $\frac{1}{3}$. This results in a different mean of λ_2 relative to that of $\{\lambda_1, \lambda_3\}$.

The CND's output with such p.d.f. is forwarded to the VND. The output of VND exhibits *asymmetry* between the LLRs for $\{w_1, w_3\}$ and w_2 . Due to such asymmetric behavior, it is not possible to characterize the EXIT function via a single-dimension representation, and hence it requires to utilize the 2-D EXIT chart curve fitting method to optimize the code degree profiles.

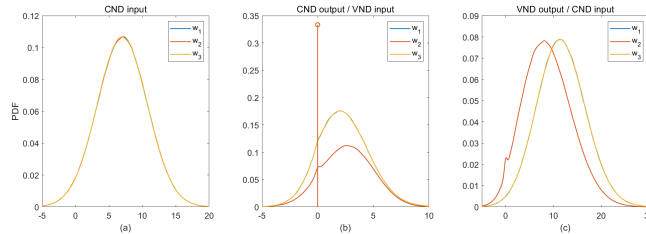


Fig. 3. PDF of LLR vectors for $m = 2$ and multipliers \mathbf{g} uniformly distributed in $\mathbb{Z}_4 \setminus \{0\}$.

D. Proposed D-IRA Can Restore the Symmetry in Soft information

Definition 2: A repeat-accumulate ring code with both irregular multiplier distribution and irregular node degree distributions is said to have a *doubly-irregular repeat accumulate* (D-IRA) structure.

So far we witnessed the impact of the zero-divisors on the asymmetry of the LLRs. One may expect that using only regular elements in the multipliers can address this issue, but this is not true. It is shown in Fig. 4 that avoiding using zero-divisors as multipliers will cause a even larger mean of λ_2 .

The idea is to exploit D-IRA structure, that is, to find the irregular multipliers distribution so that the asymmetry in the LLRs can be restored. For the $m = 2$ example, note that the fraction of the zero-divisor determines the impulse height of the p.d.f. of λ_2 at value zero. This leads to a reduced mean of λ_2 . By reducing the portion of zero-divisor 2, the mean of λ_2 can be made identical to that of λ_1 and λ_3 . It is found that the symmetric Gaussian approximation can be (approximately) restored in this manner.

For example, consider the irregular multiplier distribution of $[0.4002, 0.1996, 0.4002]$ for $g = \{1, 2, 3\}$, respectively, where the CND has a degree $d_c = 3$. The p.d.f. of the LLRs are shown in Fig. 5. Then, the output of CND is of identical means for $\{\lambda_1, \lambda_2, \lambda_3\}$. The VND output vector has (almost) identical means, even if the p.d.f. of λ_2 is not Gaussian distributed. Moreover, numerical results show that the variance of VND output LLRs also have almost identical consistent Gaussian distributions for $\{\lambda_1, \lambda_2, \lambda_3\}$. The symmetry is maintained after a complete iteration with this choice of irregular multiplier distribution. Note that as CN degree varies, the irregular multiplier distribution that restores the symmetry also varies. In the next section, this idea will be exploited to find the optimized degree profile of D-IRA ring codes.

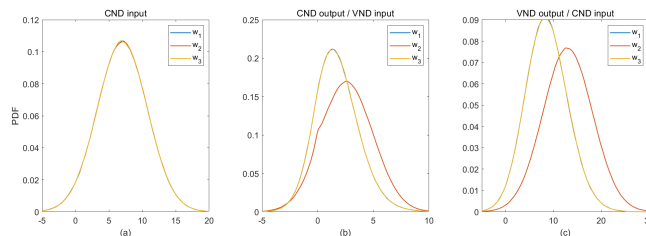


Fig. 4. PDF of LLR vectors \mathbf{g} uniformly distributed over regular elements.

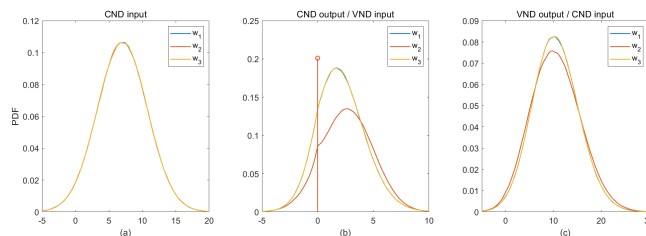


Fig. 5. PDF of LLR vectors \mathbf{g} distributed over zero-divisors and regular elements with a specific distribution. The output of CND has identical mean, and the output of VND has almost identical consistent Gaussian distribution.

IV. OPTIMIZED DESIGN OF D-IRA RING CODES FOR 2^m -PAM

In this section, we optimize the proposed D-IRA ring codes, aiming at approaching the capacity limit for any 2^m -PAM signaling. At the current stage, joint optimization of the irregular multiplier distribution

and irregular node degree distribution is a prohibitive task. We take a pragmatic approach where the optimization of these two types of distributions are decoupled.

A. Optimization of Irregular Multiplier Distribution

The non-zero elements of the integer ring, denoted by $\mathbb{Z}_{2^m} \setminus \{0\}$, is partitioned as follows. Let a subset Ω_j collect the Type- j elements in $\mathbb{Z}_{2^m} \setminus \{0\}$, given by

$$\begin{aligned}\Omega_0 &\triangleq \{a \in \mathbb{Z}_{2^m} \setminus \{0\} : M_0(a) = 2^m\}, \\ \Omega_j &\triangleq \{a \in \mathbb{Z}_{2^m} \setminus \{0\} : M_0(a) = m_j\}, j = 1, \dots, T-1\end{aligned}\quad (13)$$

where T denotes the number of types of zero-divisors. The index j is sorted according to the descending order of m_1, \dots, m_T . The cardinality $|\Omega_j|$, represents the number of different zero-divisors of type j .

Example 1: Recall the zero-divisors depicted in Table I with $2^m = 8$. The elements in \mathbb{Z}_8 are grouped into three types. The elements $\{2,6\}$ have the same zero-multiplier $M_0 = 4$, referred to as Type-I zero-divisors (or Type-I elements), where $|\Omega_1| = 2$. The element $\{4\}$ has zero-multiplier $M_0 = 2$, referred to as Type-II zero-divisor (or Type-II elements), where $|\Omega_2| = 1$. The elements $\{1,3,5,7\}$ are the regular elements whose zero-multiplier is $M_0 = 2^m$, which is referred to as Type-0 elements.

Let N_{d_c} be the total number of degree- d_c CNs. Let the multiplier distribution w.r.t. different types of zero-divisors be denoted by $\tilde{\mathbf{p}} = [\tilde{p}_0, \dots, \tilde{p}_{T-1}]^T$, where \tilde{p}_j is the probability of Type- j multipliers taking values in Ω_j , $\sum_{j=0}^{T-1} \tilde{p}_j = 1$. Due to the symmetry among the zero-divisors of the same type, the individual zero-divisors in Ω_j are allocated with equal probability. For a multiplier $a \in \Omega_j$, its probability is $\frac{\tilde{p}_j}{|\Omega_j|}$.

The basic notion of the optimization is to equalize the means of the LLRs at the CND's output for all T types of elements. With it, the symmetry of the LLRs is preserved at the VND's output shown in numerical results, which validates the EXIT curve-fitting. Let $\mathbf{\Lambda}_{in}$ be a $N_{d_c} d_c$ by $(2^m - 1)$ dimension LLR matrix as input to the CNs and $\mathbf{\Lambda}_{out}$ be that of CN output. Consider the all-zero codeword $\mathbf{c} = \mathbf{0}$ and a random coset $\boldsymbol{\theta}$. The corresponding multiplier sequence $\mathbf{g} = [g_1, \dots, g_{N_{d_c} d_c}]$ is generated according to a given distribution $\tilde{\mathbf{p}}$. Using (7), (8), the CNs' output LLR matrix $\mathbf{\Lambda}_{out}$ is obtained.

Let $\lambda_{i,j}$ be the (i, j) -th entry of matrix $\mathbf{\Lambda}_{out}$, it can be divided into partitions with $M_0(g_i)$ and $M_0(j)$. The mean matrix $\Theta = [\vartheta_{r,s}]_{T \times T}$ is calculated with

$$\vartheta_{r,s} = \{\bar{\lambda}_{i,j} \mid M_0(g_i) = m_r, M_0(j) = m_s\}. \quad (14)$$

The goal is to find a multiplier distribution so that the mean of LLR random vector $\mathbf{\Lambda}_{out}$ is equal for all types of elements. This is equivalent to finding

$$\tilde{\mathbf{p}} : \tilde{\mathbf{p}}^T \mathbf{\Theta} = \gamma \mathbf{1}_{1 \times T} \quad (15)$$

We next present an iterative algorithm to find the solution to (15) as shown in Algorithm 1 below.

Algorithm 1 Solving the optimal multiplier distribution

Require: $d_c, I_{A,CND}, \text{SNR}_{sim}$ and large enough N_c

Ensure: $\mathbf{p}_m^T \mathbf{A} = \alpha \mathbf{1}_{1 \times (T+1)}$

$p_j \leftarrow |\Omega_j| / (q - 1), j = 0, \dots, T$

$iter \leftarrow 0$

while $iter < 10$ **do**

 simulate to obtain \mathbf{A}

$\alpha \leftarrow \mathbf{p}_m^T \mathbf{A}$

$\epsilon \leftarrow (\max \alpha - \min \alpha) / \mathbb{E}[\alpha]$

$iter \leftarrow iter + 1$

if $\epsilon > 10^{-3}$ **then**

$\mathbf{p}_m^T \leftarrow \mathbf{1}_{1 \times (T+1)} \mathbf{A}^\dagger$

$\mathbf{p}_m \leftarrow \mathbf{p}_m / \sum_{j=0}^T p_j$

else

 break

end if

end while

In Algorithm 1, the initial value of \mathbf{p}_m is obtained by uniformly selecting the multiplier g from the set $\mathbb{Z}_{2^m} \setminus \{0\}$. Note that this initial value can also be replaced by other empirical values, which may speed up the convergence of the algorithm. $\mathbf{\Theta}^\dagger$ denotes the Moore-Penrose inverse of $\mathbf{\Theta}$. The updated value of \mathbf{p}_m may be of negative entry, which will be forced to 0. In this case, the i -th row of $\mathbf{\Theta}$ corresponding to $p_i = 0$ are all zeros. The solution obtained by Moore-Penrose inverse is the least square solution [27]. When there is no \mathbf{p}_m that meets $\mathbf{p}_m^T \mathbf{\Theta} = \alpha \mathbf{1}_{1 \times (T+1)}$, the obtained solution ensures that the difference among the entries of $\mathbf{p}_m^T \mathbf{\Theta}$ are minimized.

With the optimized irregular multiplier distribution, numerical results show that the symmetric Gaussian approximation is maintained well. As such, the optimization of the irregular node degree distribution with EXIT chart is in line with the trajectory of mutual information in the iterative decoding process.

B. Computation of EXIT Functions

Here we characterize input-output mutual information (MI), i.e. the EXIT functions [28], of VN and CN of the D-IRA ring codes. The utilization of random coset has the same effect as the output symmetry of binary LDPC codes [29]–[32]. The EXIT function of VN with degree d_v is given by [4], [28]

$$I_{E,VND}(I_A, d_v) = J((d_v - 1) \cdot J^{-1}(I_A)) \quad (16)$$

where $J(\sigma^2) = I(C; \Lambda)$ denotes the MI between the genuine codeword and the LLR sequence, which is characterized with a single-parameter σ^2 . For CNs, if the distribution of the output LLR vector satisfies

$$\Pr[\lambda | C = \omega] = \Pr[\lambda^{+\omega} | C = 0], \quad (17)$$

i.e., the symmetric condition is met, then the (normalized) mutual information can be expressed as

$$I(C; \Lambda) = 1 - \mathbb{E} \left[\log_{2^m} \left(1 + \sum_{i=1}^{2^m-1} e^{-\lambda_i} \right) \right]. \quad (18)$$

The operator $\mathbb{E}[\cdot]$ denotes the expectation over the LLR vectors, which can be approximated numerically in practice. In this paper, we use the assumption in (17). This avoids multi-dimensional integration in the calculation of mutual information and yield a satisfactory performance as we will see later.

For edges with multiplier of zero-divisors, the output probabilities are block-wisely repeated. If the zero-multiplier M_0 of the zero divisor is m_j , the first $(m_j - 1)$ entries of Λ contains all information, i.e.,

$$\begin{aligned} I(C; \Lambda_{1:m_j-1}) &= 1 - \mathbb{E} \left[\log_{2^m} \left(1 + \sum_{i=1}^{m_j-1} e^{-w_i} \right) \right] = 1 - \mathbb{E} \left[\log_{2^m} \left(\frac{2^m}{m_j} \left(1 + \sum_{i=1}^{m_j-1} e^{-w_i} \right) \right) \right] \\ &= 1 - \mathbb{E} \left[\log_{2^m} \left(1 + \sum_{i=1}^{2^m-1} e^{-w_i} \right) \right], \end{aligned} \quad (19)$$

where the equality in the last step is due to the block-wise repetition of probabilities.

For CNs with degree d_c , the output mutual information normalized by $\log_2 2^m$ is obtained by

$$I_{E,CND}(I_A; d_c, \sigma_z^2) = 1 - \mathbb{E} \left[\log_{2^m} \left(1 + \sum_{i=1}^{2^m-1} e^{-\lambda_i} \right) \right] \quad (20)$$

where the input LLR vectors obey the joint Gaussian distribution [33] with parameter σ^2 meeting $J(\sigma^2) = I_A$, the AWGN variance is σ_z^2 . For $I_A = 1$, we have $\sum_{i=1}^{m_j-1} e^{-\lambda_i} = 0$ and

$$I_{E,CND}(I_A = 1; d_c, \sigma_z^2) = \frac{1}{\log_2 2^m} \sum_{j=0}^T p_j \log_2(m_j) < 1, \quad (21)$$

according to the first equality in (19).

C. Optimization of Irregular Node Degree Distribution

The distribution of node degrees is defined by polynomials

$$\varphi(x) = \sum_{i=2}^{D_v} \varphi_i x^{i-1} \text{ and } \rho(x) = \sum_{j=1}^{D_c} \rho_j x^{j-1}, \quad (22)$$

where D_v and D_c denote the maximum degree of VNs and CNs respectively, λ_i denotes the fraction of edges connected to variable nodes with degree i and ρ_j denotes that of check nodes with degree j . The coding rate w.r.t. (φ, ρ) is

$$R_s = \frac{\sum_{i=2}^{D_v} \varphi_i / i}{\sum_{j=1}^{D_c} \rho_j / j}. \quad (23)$$

For given degree distribution (φ, ρ) , the effective EXIT functions are

$$\begin{aligned} I_{E,VND}(I_A) &= \sum_{i=2}^{D_v} \lambda_i I_{E,VND}(I_A; i) \\ I_{E,CND}(I_A; \sigma_z^2) &= \sum_{j=1}^{D_c} \rho_j I_{E,CND}(I_A; j, \sigma_z^2). \end{aligned} \quad (24)$$

For a given degree distribution of CNs, we utilize linear programming to optimize the degree distribution of VNs. The constraints are (23) and

$$I_{E,VND}(I_A) > I_{E,CND}^{-1}(I_A; \sigma_z^2), \quad 0 \leq I < 1. \quad (25)$$

For given degree distribution of VNs, the constraint (25) becomes

$$I_{E,CND}(I_A; \sigma_z^2) > I_{E,VND}^{-1}(I_A), \quad 0 \leq I < 1. \quad (26)$$

The algorithm for optimizing the node degree distribution is shown in **Algorithm 2**. In Algorithm 2,

Algorithm 2 Solving the optimal node degree distribution

Require: R_s , $I_{E,VND}(I_A; d_v)$ and $I_{E,CND}(I_A; d_c, \sigma_z^2)$

Ensure: expressions (23), (25), (26) with $I_{A,CND} \in [0, 0.85]$

$\rho^{(0)} : (\rho_1, \rho_3) \leftarrow (0.1, 0.9)$

$n \leftarrow 1$

while $n < 10$ **do**

 use $\rho^{(n-1)}$, $I_{E,CND}(I_A; d_c, \sigma_z^2)$ to get $I_{A,CND}(I_E; \sigma_z^2)$

$\lambda^{(n)} \leftarrow \arg \max_{\lambda} \left(\min \left(\frac{I_{E,VND}(I_A) - I_{A,CND}(I_E; \sigma_z^2)}{\sqrt{1 + I'_{A,CND}(I_E; \sigma_z^2)^2}} \right) \right)$

 use $\lambda^{(n)}$, $I_{E,VND}(I_A; d_v)$ to get $I_{A,VND}(I_E)$

$\rho^{(n)} \leftarrow \arg \max_{\rho} \left(\min \left(\frac{I_{E,CND}(I_A; \sigma_z^2) - I_{A,VND}(I_E)}{\sqrt{1 + I'_{A,VND}(I_E)^2}} \right) \right)$

$n \leftarrow n + 1$

end while

$I_A(I_E)$ denotes the inverse function $I_E^{-1}(I_A)$ and $I'_A(I_E)$ denotes its derivative. This algorithm is set to maximize the narrowest gap between the two EXIT curves.

D. Partially Random Interleaver

Here we introduce the partially random interleaver of the D-IRA ring codes. With the optimized multiplier distribution and node degree distribution, the edges of CNs and the associated multipliers are

determined. The interleaver connects these edges to the VNs with a specific order [34] [35]. According to the degrees of CNs and VNs and the multipliers, the edges are divided into two categories.

(i) For degree-2 and 3 VNs, the edges have multipliers of regular elements (no zero-divisors).

(ii) For VN with degree greater than 3, the edges are allowed to have zero-divisors. The number of edges with zero-divisors cannot exceed a certain proportion of its node degree (e.g., 1/3).

Then, the edges of VNs are randomly connected subject to the above constraint, and hence the name “partially random” interleaver. By and large, the edges of multipliers of zero-divisors are connected to VNs of large degrees. This can effectively reduce the effect of the ambiguity due to the multipliers of zero-divisors in the LLR calculation of the CNs.

E. Check Nodes with Degree One are no Longer Required

In existing IRA codes over Galois fields, a portion of $d_c = 1$ CNs must be used. For example in [4], 20% of the CNs are forced to have degree 1. This is due to that the input mutual information obtained purely from the channel intrinsic information is zero for $d_c \geq 2$ CNs, and the iterative decoding process cannot commence without degree-1 CNs. This part will show that in D-IRA ring codes such requirement is relaxed. As such, the tunnel between the EXIT curves may be better exploited.

Lemma 1: Consider a CN with at least one input edge whose multiplier is a regular element. If the input vector w.r.t. the regular element has equal probability, the output vector also has equal probability.

Proof. When g is a regular element, $\mathbf{x}^{\times g}$ in (46) is an arrangement of \mathbf{x} . Without losing generality, the k -th input edge is labeled with regular element and has equiprobable probability vector \mathbf{r}^k . So there is $\bar{\mathbf{r}}^k = \left[\frac{1}{q}, \dots, \frac{1}{q}\right]$ and $\text{DFT}(\bar{\mathbf{r}}^k) = [1, 0, \dots, 0]$. The first element of the DFT vector is the sum of the probability vector, which is 1 for all input edges. According to (47), the output is

$$\bar{\mathbf{l}} = \text{IDFT}([1, 0, \dots, 0]) = \left[\frac{1}{q}, \dots, \frac{1}{q}\right]. \quad (27)$$

Because every element in \mathbf{l} is an element in $\bar{\mathbf{l}}$, the output probability vector is also equal probability. ■

Consider a CN with $d_c > 1$. This CN has the constraint equation $\sum_{n=1}^{d_c+2} h_n a_n = 0$. Consider the initial state, i.e. $I_{A,CND} = 0$. That is, the initial probability vector $\mathbf{r}^n = \left[\frac{1}{2^m}, \dots, \frac{1}{2^m}\right]$, $n = 1, \dots, d_c$. If there is at least one regular element in the multipliers h_1, \dots, h_{d_c} , the output probability vectors $\mathbf{l}^{d_c+1} = \left[\frac{1}{2^m}, \dots, \frac{1}{2^m}\right]$ and $\mathbf{l}^{d_c+2} = \left[\frac{1}{2^m}, \dots, \frac{1}{2^m}\right]$ according to Lemma 1.

\mathbf{l}^{d_c+1} and \mathbf{l}^{d_c+2} are also equiprobable for the previous or next CN, so \mathbf{r}^{d_c+1} and \mathbf{r}^{d_c+2} are equal to the probability vectors of the channel, which are \mathbf{p}^1 and \mathbf{p}^2 respectively. Let \mathbf{Fp} denote the product of the a

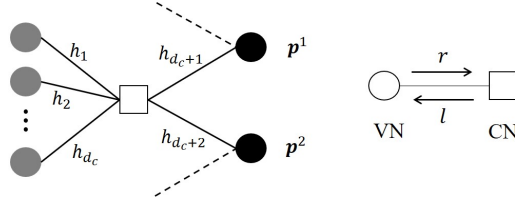


Fig. 6. Illustration of a CN of degree d_c and the multipliers.

posteriori probability vector from the channel

$$\mathbf{Fp} = \text{DFT}(\bar{\mathbf{p}}^1) \cdot \text{DFT}(\bar{\mathbf{p}}^2) \quad (28)$$

where $\bar{\mathbf{p}}^1$ and $\bar{\mathbf{p}}^2$ are the multiplication cycles with $h_{d_c+1}^{-1}$ and $h_{d_c+2}^{-1}$ respectively.

Consider the output probability vectors of CN. If there are two or more regular elements in the multipliers h_1, \dots, h_{d_c} , all of the output vectors are equal probability according to Lemma 1, that is, $I_{E,CND} = 0$. There is $I_{E,CND} > 0$ only when the check node with degree d_c has at least $d_c - 1$ zero-divisors.

As multipliers of the same check node should avoid too many zero-divisors, we consider the CN with degree 2 here. Suppose h_1 is a regular element and h_2 is a zero divisor. \mathbf{l}^2 is equiprobable and

$$\bar{\mathbf{l}}^1 = \text{IDFT}(\text{DFT}(\bar{\mathbf{r}}^2) \cdot \mathbf{Fp}). \quad (29)$$

The DFT vector of the multiplication cycle of the probability vector is dual to the multiplication cycle of the DFT vector of the probability vector, that is

$$\begin{aligned} \text{DFT}(\bar{\mathbf{r}}^2) &= (\text{DFT}(\mathbf{r}^2))^{\times(-h_2)} = ([1, 0, \dots, 0])^{\times(-h_2)} \\ &= \begin{cases} 1 & i \otimes h_2 = 0 \\ 0 & i \otimes h_2 \neq 0 \end{cases}. \end{aligned} \quad (30)$$

The zero-multiplier of h_2 is $M_0(h_2) < q$. So at least two elements in the DFT vector are 1.

According to (20), the mutual information corresponding to an edge can be rewritten as

$$1 - \log_{2^m} \left(1 + \sum_{i=1}^{q-1} e^{-\lambda_i} \right) = 1 + \log_{2^m}(p_0) \quad (31)$$

That is, the output mutual information is only related to the zeroth element of the probability vector.

According to the IDFT calculation,

$$l_0^1 = \bar{l}_0^1 = \frac{1}{2^m} \sum_{i=0}^{2^m-1} [\text{DFT}(\bar{\mathbf{l}}^1)]_i \quad (32)$$

Therefore, the mutual information of the edge corresponding to l^2 is 0 and that corresponding to l^1 is

$$1 + \log_{2^m} (l_0^1) = \log_{2^m} \left(\sum_{i=0}^{q/M_0(h_2)-1} [\mathbf{F}\mathbf{p}]_{i \cdot M_0(h_2)} \right) \quad (33)$$

The above expressions are the same for multipliers with the same M_0 , so the corresponding MI is

$$I_E(m_j, \sigma_z^2) = \mathbb{E} \left[\log_{2^m} \left(\sum_{i=0}^{2^m/m_j-1} [\mathbf{F}\mathbf{p}]_{i \cdot m_j} \right) \right] \quad (34)$$

where $m_0 = 2^m$ and $I_E(m_0, \sigma_z^2) = 0$ include the case that h_2 is a regular element.

For CNs with $d_c = 2$, if there is at least one regular element, the initial output MI is

$$I_{E,CND}(I_A = 0; d_c = 2, \sigma_z^2) = \sum_{j=1}^T p_j I_e(m_j, \sigma_z^2). \quad (35)$$

If the multiplier takes more zero-divisors (especially the zero-divisors with smaller M_0), the initial output mutual information of the CN with degree 2 is non-zero which enables the commencement of iterative decoding. Therefore, CNs with degree 1 is no longer required. We conjecture that the performance improvement of D-IRA ring codes (to be shown in the numerical result section) is due to the relaxation of the requirement of degree-1 CNs.

V. D-IRA RING CODES FOR MULTI-USER NETWORKS

We now turn to our real interest: to exploit structured binning with D-IRA ring codes in multi-user networks, with practical 2^m -PAM signaling. Here we only present the treatment for the CF and DPC setups, which can be extended to other network configurations. The techniques presented in this section do not apply for conventional BICM, SCM, TCM and existing $\text{GF}(2^m)$ modulation codes.

A. D-IRA Ring codes for Compute-forward

Let $\mathbf{w}_1, \dots, \mathbf{w}_K$ denote the 2^m -ary message sequences of the K users. Each user's message sequence is encoded as in (1) via a common D-IRA ring code, yielding coded sequences $\mathbf{c}_1, \dots, \mathbf{c}_K$. Let $\mathbf{x}_1, \dots, \mathbf{x}_K$ denote the resultant 2^m -PAM sequences after the one-to-one mapping in (2), which are transmitted simultaneously. The received signal is

$$\mathbf{y} = \sum_{i=1}^K h_i \mathbf{x}_i + \mathbf{z}. \quad (36)$$

where h_i denotes the channel gain of user i . The receiver aims to compute L linear message combinations

$$\mathbf{u}_l \triangleq \alpha_{l,1} \mathbf{w}_1 \oplus \alpha_{l,2} \mathbf{w}_2 \oplus \dots \oplus \alpha_{l,K} \mathbf{w}_K, l = 1, \dots, L \quad (37)$$

where $\alpha_{l,1}, \dots, \alpha_{l,K} \in \mathbb{Z}_{2^m}$ are the coefficients. Let $\boldsymbol{\alpha}_l = [\alpha_{l,1}, \dots, \alpha_{l,K}]^T$ be a *coefficient vector*, and let $\mathbf{A} = [\boldsymbol{\alpha}_1, \dots, \boldsymbol{\alpha}_L]^T$ be the *coefficient matrix*.

We note that CF or linear PNC is not only confined to the toy example of two-way relay channel studied in the early stage of this subject. It is now understood that CF or linear PNC applies to a wide range of multi-user communication configurations, such as multiple-access (MA), broadcast (BC), distributed MIMO, integer-forcing (IF) MIMO detection, IF precoding, interference alignment, multi-access relay and etc., with remarkable advances in achievable rates [14], [16], [20], [36]. As such, we consider the above model that consists of K users and one receiver, where the receiver is set to compute L linear message combinations. Such a model is the core to any systems operated with CF. For the case of $K = 2$, $L = 1$, the model can be used to represent the uplink phase of a two-way relay channel. For the case of $L = K$, when coefficient matrix \mathbf{A} is invertible over \mathbb{Z}_{2^m} , the model can be used to represent an uplink MA system. The subsequent operations, such as the downlink phase of the two-way relay channel and the multiplication of the inverse of the channel coefficient matrix in MA and distributed MIMO, are diverse and thus not presented in this paper. Interested readers may find the details in [10], [20].

1) *Structured Binning*: Here, a certain \mathbf{u}_l specifies a set of candidates $[\mathbf{w}_1, \dots, \mathbf{w}_K]$ of the same underlying linear message combination, which is essentially a “*bin-index*” in the jargon of network information theory. In particular, the bin-index \mathbf{u}_l is given by a linear structure specified in (37), hence the name “*structured binning*”. Apparently, different choice of coefficient vectors yield different binning structures. Roughly speaking, the L coefficient vectors with the “best” binning structures, such that the bin-indices can be most reliably computed, should be selected and utilized.

Traditional non-PNC schemes completely decodes $\mathbf{w}_1, \dots, \mathbf{w}_K$ individually, and then form \mathbf{u}_l . These schemes are based on the notion of *random coding* for the multi-user communication. With lattice codes or ring codes, PNC can exploit structured binning to directly computes \mathbf{u}_l without the complete decoding, yielding significant coding or even multiplexing gain. CF characterizes the achievable rate for reliably computing of \mathbf{u}_l based on the existence of good lattice codes for structured binning. The implementation of a D-IRA ring coded PNC system is depicted as follows.

Let $\mathbf{C} = [\mathbf{c}_1, \dots, \mathbf{c}_K]^T$ stacks up all users’ coded sequences generated by the D-IRA ring code. Define

$$\mathbf{v}_l^T \triangleq \text{mod} \left(\sum_{i=1}^K a_{l,i} \mathbf{c}_i^T, q \right) = \mathbf{a}_l^T \otimes_q \mathbf{C} \quad (38)$$

as the l -th “*linear coded-sequence combination*”.

Property 2: With the generator matrix \mathbf{G} in (1), we have

$$\begin{aligned} \mathbf{v}_l &= \text{mod} \left(\sum_{i=1}^K a_{l,i} \mathbf{G} \otimes_q \mathbf{b}_i, q \right) = \mathbf{G} \otimes_q \text{mod} \left(\sum_{i=1}^K a_{l,i} \mathbf{b}_i, q \right) \\ &= \mathbf{G} \otimes_q \mathbf{u}_l. \end{aligned} \quad (39)$$

That is, a linear coded-sequence combination \mathbf{v}_l and a linear message combination \mathbf{u}_l are also related by the multiplication of \mathbf{G} modulo- q .

Property 2 allows for: 1) calculating the symbol-wise APPs of \mathbf{v}_l over the extended constellation, to be detailed momentarily; 2) forward the resultant APP sequence to a decoder to compute \mathbf{u}_l . We note that such treatment is impossible for non-lattice code based schemes where Properties 2 does not hold. The implementation of 1) and 2) are illustrated below:

Let $v_l[t]$ and $y[t]$ denote the t -th column of \mathbf{v}_l and \mathbf{y} , respectively. The receiver calculates the symbol-wise APPs of the linear coded-sequence combinations $p(v_l[t] | y[t])$. This can be implemented in parallel or in succession for $l = 1, \dots, L$. Using the Baye's rule, we obtain

$$p(v_l[t] = \omega | y[t]) = \sum_{\substack{x_1[t], \dots, x_K[t]: \\ \mathbf{a}_l^T \otimes \mathbf{c}[t] = \omega}} p \left(y[t] | \sum_{i=1}^K h_i x_i[t] \right), \omega = 0, \dots, 2^m - 1. \quad (40)$$

It equals to the sum of the likelihood functions of the 2^m candidates in the bin with index ω . The APPs are forwarded to L D-IRA ring code BP decoders, which yield decision on \mathbf{u}_l , $l = 1, \dots, L$, in the case with parallel computing. More details, such as successive computing, can be found in [10], [17].

2) *D-IRA Ring Code Optimization:* The optimized design of the D-IRA ring codes for this CF setting needs to evaluate the input-output mutual information transfer function that takes into account the symbol-wise APP calculation over the extended constellation depicted above. In particular, such operation result in a varied EXIT function for the combined check-accumulator. Thus, the curve-fitting of the EXIT functions need to adapt to these change in generating the optimized D-IRA ring code degree-profile. For the CF setting, it is empirically found that a good single-user D-IRA ring code tends to be a good code for the K -user CF setting as well, as we will shown in the numerical result section.

Remark 1: The zero-divisors can also be used as coefficients in certain setups. For MA where $L = K$, it can be shown that as long as $\text{mod}(|\mathbf{A}|, q)$ is a regular element, all users' message can be recovered.

B. D-IRA Ring codes for Linear Dirty Paper Coding

Consider the DPC setting where a base station (BS) wants to deliver a message to a user equipment (UE), subject to some interference at the UE receiver [37]. Let \mathbf{w} denote the 2^m -ary message sequence

and \mathbf{x} denote the coded 2^m -PAM signal sequence transmitted by BS. The UE receives

$$\mathbf{y} = \mathbf{x} + \mathbf{s} + \mathbf{z} \quad (41)$$

where \mathbf{s} is the interference and \mathbf{z} is the additive white Gaussian noise (AWGN) of mean zero and variance σ^2 . The interference \mathbf{s} is known by the BS transmitter but not by the UE receiver. For applications in the downlink of cellular network, \mathbf{s} could be the signal to another UE. It is well-known that DPC is required to achieve the capacity of this multi-source channel.

For the clarity of presentation, let us omit the power normalization factor γ in (2). For integer interference, i.e., $\mathbf{s} \in \mathbb{Z}^n$, a simple linear DPC method is given by [38]

$$\mathbf{x} = \mathbf{c} \ominus \mathbf{s} - \frac{q-1}{2} \quad (42)$$

where $a \ominus b = \text{mod}(a - b, 2^m)$. Integer interference arises when \mathbf{s} is a PAM signal from another UE. The treatment for non-integer \mathbf{s} can be found in [38], and is not presented in this paper due to space limitation.

The UE receiver does not know \mathbf{s} , but has knowledge on the statistics, e.g. the p.m.f. or p.d.f. of \mathbf{s} . Let

$$\mathbf{r} = \mathbf{x} + \mathbf{s} \quad (43)$$

denote the signal plus interference (without noise) at UE receiver. With (41) and (42), we obtain

$$\mathbf{r} = \mathbf{c} \ominus \mathbf{s}_Q + \mathbf{s}_Q - \frac{q-1}{2} \quad (44)$$

which is guaranteed to belong to an extended codebook of the ring code [38]. This does not hold for the $\text{GF}(2^m)$ codes [9]. The receiver is set to compute the bin-index with the following procedures:

1) Upon receiving \mathbf{y} in (41), compute the symbol-wise APPs w.r.t. the entries of the coded sequence \mathbf{c} . For the t th symbol, $t = 1, \dots, n$, the APP for $c[t] = i$, $i = 0, \dots, 2^m - 1$, is

$$\begin{aligned} p(c[t] = i | y[t]) &= \sum_{r[t] \in \overline{\mathbb{C}}(i)} p(r[t] | y[t]) \propto \sum_{r[t] \in \overline{\mathbb{C}}(i)} p(y[t] | r[t]) p(r[t]) \\ &= \frac{1}{\beta} \sum_{r[t] \in \overline{\mathbb{C}}(i)} \exp\left(-\frac{(y[t] - r[t])^2}{2\sigma^2}\right) p(r[t]) \end{aligned} \quad (45)$$

where β is a normalization factor to ensure $\sum_{i=0, \dots, q-1} p(c[t] = i | y[t]) = 1$, $\overline{\mathbb{C}}(i)$ denotes the extended constellation of 2^m -PAM. The a priori probability of $p(r[t])$ is obtained from the statistics of \mathbf{s} [38].

2) The APPs are forwarded to the D-IRA BP decoder, which yields the decoding output $\hat{\mathbf{w}}$.

The optimized design of D-IRA ring codes for DPC utilizes the input-output MI transfer function that

takes into account the DPC channel and symbol-wise APP soft detector. Then, the optimization for the irregular-degree multiplier and irregular node degree distributions follows the procedures in Sections III and IV, Algorithms I and II. Our optimized solution for the D-IRA ring coded DPC is given in Table. II.

TABLE II
OPTIMIZED DEGREE PROFILE OF D-IRA RING CODES FOR DPC.

	Repeat Node Degree	Combiner Node Degree	Distribution of Multipliers
$q=4$ Rate= $1/2$	$0.0008x^2+0.779x^3+0.0718x^9$ $+0.1097x^{12}+0.0256x^{20}+0.0131x^{60}$	$0.084x+0.0344x^2$ $+0.8804x^3+0.0012x^5$	$[p_1, p_2, p_3]=[0.4856, 0.1657, 0.3487]$
$q=8$ Rate= $1/2$	$0.3646x^2+0.3927x^3+0.019x^6+0.0064x^8$ $+0.1674x^{10}+0.0292x^{28}+0.0207x^{50}$	$0.084x+0.0991x^2$ $+0.7499x^3+0.0671x^4$	$[p_1, \dots, p_7]=[0.2032, 0.0882, 0.2032$ $0.0107, 0.2032, 0.0882, 0.2032]$
$q=8$ Rate= $2/3$	$0.4260x^2+0.3915x^3+0.0395x^6+0.0898x^9$ $+0.0318x^{12}+0.0171x^{32}+0.0043x^{60}$	$0.0284x+0.2016x^2$ $+0.7208x^3+0.0492x^5$	$[p_1, \dots, p_7]=[0.2226, 0.0467, 0.2226$ $0.0162, 0.2226, 0.0467, 0.2226]$
$q=16$ Rate= $5/8$	$0.6402x^2+0.0888x^3+0.0626x^4+0.1175x^6$ $+0.0481x^{12}+0.0257x^{21}+0.017x^{60}$	$0.0401x+0.061x^2$ $+0.0858x^3+0.012x^4$	$[p_1, \dots, p_{15}]=[0.1196, 0.0071, 0.1196,$ $0.0053, 0.1196, 0.0071, 0.1196,$ $0.0041, 0.1196, 0.0071, 0.1196,$ $0.0053, 0.1196, 0.0071, 0.1196,]$

We note that the ring coded linear DPC generally outperforms binary coded DPC. To be specific, ring coded linear DPC follows the notion of vector quantization over lattices, and can be shown to minimize the quantization error as q increases. In contrast, a binary coded DPC is implemented based on the soft probabilities w.r.t. the binary codes by dealing with the many-to-one constellation mapping, which give rises to a performance gap to the ring coded DPC, as will be shown in the numerical result section.

VI. DESIGN EXAMPLES AND NUMERICAL RESULTS

A. D-IRA Ring Codes for Point-to-point AWGN Channel

This part presents the optimized code profile of D-IRA ring codes for AWGN channel. For $q = 4$, the coding rates under consideration are $R_c = 1/4, 1/2, 3/4$, where the spectral efficiency are $R = 1/2, 1, 3/2$ respectively. For $q = 8$, the coding rates under consideration are $R_c = 1/3, 1/2, 2/3$, where the spectral efficiency are $R = 1, 3/2, 2$ respectively. The capacity limits w.r.t. these rates are obtained by evaluating the mutual information with 4-PAM and 8-PAM channel inputs.

TABLE III
THE MULTIPLIER DISTRIBUTION FOR $q = 4$.

	R=0.5		R=1.0		R=1.5	
1	0.8420	0.1580	0.7965	0.2035	0.7223	0.2777
2	0.8222	0.1778	0.8115	0.1885	0.8507	0.1493
3	0.8022	0.1978	0.8004	0.1996	0.8610	0.1390
4	0.7885	0.2115	0.7921	0.2079	0.8661	0.1339
5	0.7773	0.2227	0.7855	0.2145	0.8693	0.1307
6	0.7693	0.2307	0.7799	0.2201	0.8715	0.1285
Ω	{1, 3}	{2}	{1, 3}	{2}	{1, 3}	{2}

The optimized irregular multiplier distribution for $q = 4$ is shown in TABLE III, which is obtained by utilizing Algorithm 1. For each rate, the portion of multipliers with coefficients {1,3} is given by the

TABLE IV
THE NODE DEGREE DISTRIBUTION FOR $q = 4$.

R=0.5	$\varphi(x) = 0.1611x^3 + 0.0402x^9 + 0.1910x^{11} + 0.1104x^{12} + 0.4877x^{47} + 0.0096x^{49}$ $\rho(x) = 0.0367x^1 + 0.5490x^2 + 0.0285x^5 + 0.3858x^6$
R=1.0	$\varphi(x) = 0.0800x^2 + 0.1492x^3 + 0.2379x^4 + 0.0101x^9 + 0.2384x^{10} + 0.1657x^{13} + 0.1187x^{22}$ $\rho(x) = 0.0080x^1 + 0.5012x^2 + 0.2532x^3 + 0.0239x^4 + 0.2136x^6$
R=1.5	$\varphi(x) = 0.2187x^2 + 0.3363x^3 + 0.1576x^4 + 0.0692x^9 + 0.1605x^{10} + 0.0363x^{14} + 0.0214x^{17}$ $\rho(x) = 0.3658x^2 + 0.5649x^3 + 0.0223x^4 + 0.0470x^6$

column on the left, while that with coefficients $\{2\}$ is given by the column on the right. Each row denotes the portions of multipliers for a specific CN degree, where the maximum CN degree is set to 6. For example, for the spectral efficiency of 1 bits/symbol per real-dimension, for CN of degree 2, 18.85% of the multipliers are $\{2\}$ while 81.15% of the multipliers are either $\{1\}$ or $\{3\}$. The multipliers with the same M_0 have identical portion, e.g., multipliers $\{1\}$ has portion 40.575% while multipliers $\{3\}$ has portion 40.575%. We note that certain amount of multiplier with zero-divisor $\{2\}$ helps with the convergence behavior and the decoding performance, relative to that without using a zero-divisor in the multipliers. The ambiguity brought about by the zero-divisor multiplier can be addressed in the BP decoding with the help from other nodes of different multipliers and the partially random interleaver. As the rate increases, less portion of multipliers with zero-divisor $\{2\}$ is allocated. This can be explained by considering that as the coding rate approaches 1, there will be no redundancy digits and hence the zero-divisor $\{2\}$ incurs ambiguity in the division which cannot be solved. The node degree distribution is shown in Table. IV. The polynomial λ denotes the degree distribution of the information (or repetition) nodes, while polynomial ρ denotes the degree distribution of the CNs. The solution is obtained by utilizing Algorithm 2.

TABLE V
THE MULTIPLIER DISTRIBUTION FOR $q = 8$.

	R=1.0			R=1.5			R=2.0		
1	0.7506	0.2190	0.0304	0.6796	0.2571	0.0633	0.6971	0.2156	0.0872
2	0.7549	0.2122	0.0329	0.7857	0.1734	0.0409	0.8700	0.0000	0.1300
3	0.7336	0.2191	0.0473	0.7871	0.1573	0.0556	0.8684	0.0000	0.1316
4	0.7153	0.2240	0.0607	0.7840	0.1463	0.0696	0.8642	0.0000	0.1358
5	0.7007	0.2275	0.0718	0.7803	0.1380	0.0816	0.8592	0.0000	0.1408
6	0.6893	0.2303	0.0804	0.7776	0.1301	0.0924	0.8546	0.0000	0.1454
Ω	$\{1, 3, 5, 7\}$	$\{2, 6\}$	$\{4\}$	$\{1, 3, 5, 7\}$	$\{2, 6\}$	$\{4\}$	$\{1, 3, 5, 7\}$	$\{2, 6\}$	$\{4\}$

The optimized irregular multiplier distribution for $q = 8$ is shown in TABLE V. For each rate in the design, the portion of multipliers with coefficients $\{1,3,5,7\}$ is given by the column on the left, while that with coefficients $\{2,6\}$ is given by the column in the middle, that those with $\{4\}$ is given by the column on the right. In this example, there are two types of zero-divisors: $\{2,6\}$ and $\{4\}$. For a relatively high rate, e.g., spectral efficiency of 2 bits/symbol per real-dimension, the portion of multipliers with zero-multiplier

TABLE VI
THE NODE DEGREE DISTRIBUTION FOR $q = 8$.

R=1.0	$\varphi(x) = 0.0600x^2 + 0.1064x^3 + 0.1113x^5 + 0.1442x^8 + 0.1442x^{13} + 0.0915x^{25} + 0.0248x^{26} + 0.3175x^{57}$ $\rho(x) = 0.0175x^1 + 0.5990x^2 + 0.0054x^5 + 0.3781x^6$
R=1.5	$\varphi(x) = 0.0955x^2 + 0.2464x^3 + 0.2510x^7 + 0.0615x^8 + 0.0824x^{10} + 0.1584x^{24} + 0.1047x^{26}$ $\rho(x) = 0.0180x^1 + 0.5000x^2 + 0.2161x^3 + 0.0078x^5 + 0.2580x^6$
R=2.0	$\varphi(x) = 0.2103x^2 + 0.1852x^3 + 0.3199x^6 + 0.1124x^{17} + 0.0746x^{21} + 0.0976x^{48}$ $\rho(x) = 0.0004x^1 + 0.1500x^2 + 0.7856x^3 + 0.0078x^4 + 0.0561x^6$

coefficient $\{2,6\}$ becomes zero except for $d_c = 1$. For a relatively low rate, the portion of multipliers with zero-multiplier coefficient $\{2,6\}$ is significantly greater than that for $\{4\}$. The irregular node degree distribution obtained from Algorithm 2 is shown in Table. VI.

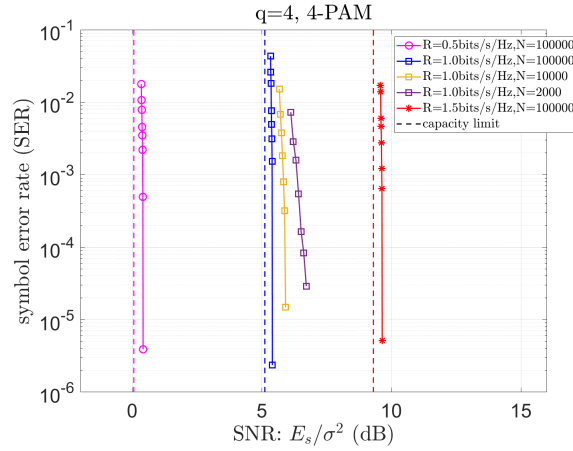


Fig. 7. Performance of $q = 4$ D-IRA ring codes with 4-PAM and various coding rates.

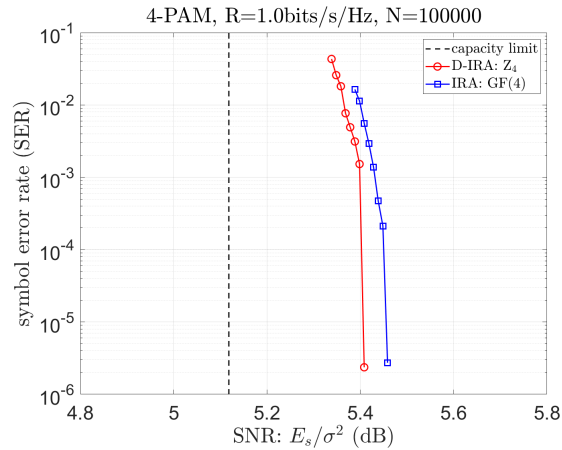


Fig. 8. Performance comparison of D-IRA ring codes and GF(4) IRA modulation codes with 4-PAM.

Fig. 7 shows the error-rate performance of the optimized D-IRA ring coded q -PAM scheme of $q = 4$, with the designed code profiles given in the above. The codeword length is set to $n = 100000$. At SER of 10^{-5} , the gaps between the symbol error performance of the optimized D-IRA ring code and the capacity limits of 4-PAM are only 0.36, 0.29, 0.34 dB for spectral efficiencies of $R = 1/2, 1, 3/2$, respectively. In Fig. 8, we plot the error rate performance of the modulation code based on GF(4) with optimized degree

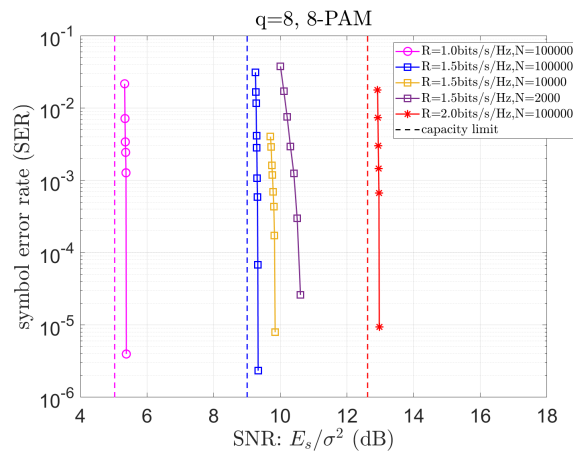


Fig. 9. Performance of $q = 8$ D-IRA ring codes with 8-PAM and various coding rates.

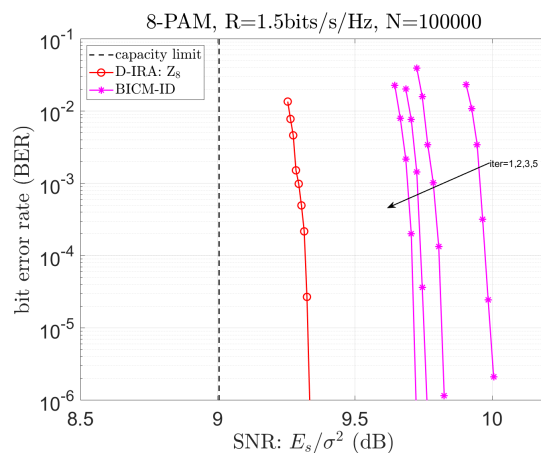


Fig. 10. Performance comparison of D-IRA ring codes and Gray mapping BICM-ID with different iterations with 8-PAM.

profile reported in [9]. It is observed that the proposed D-IRA ring code, optimized via the pragmatic algorithms, exhibits a performance advantage of 0.05 dB at spectral efficiency of $R = 1$. We conjecture that this is primarily due to the fact that the existing binary and q -ary codes over Galois fields require a portion of $d_c = 1$ check nodes, otherwise the iterative decoding will not commence. In contrast, in the proposed D-IRA ring codes, even without $d_c = 1$ CNs, the iterative process can still start, owing to the existence of multipliers of zero-divisors. This may give rise to further narrowed gap between the EXIT curves. At the current stage, there is still no rigorous proof for this performance advantage.

Fig. 9 shows the performance of D-IRA ring codes for $m = 3$ (or $q = 8$). At SER of 10^{-5} , the gaps between the optimized D-IRA modulation code and the capacity limits of 8-PAM are only 0.35, 0.33, 0.35 dB for $R = 1, 3/2, 2$, respectively. We also compare to existing BICM-ID scheme with three levels of binary codes in Fig. 10. It is observed that the proposed D-IRA ring code yields 0.7 dB and 0.4 dB performance advantages over the competing scheme with 1 and 5 BICM-ID iterations, respectively.

Fig. 7 and Fig. 9 also show the performance of D-IRA ring codes for $q = 4, R = 1.0$ and $q = 8, R =$

1.5 with different codeword lengths. The ring codes with different lengths adopt the same multiplier distribution and node degree distribution according to TABLE III-VI. At SER of 10^{-5} , the gaps between the optimized D-IRA modulation code and the capacity limits of 4-PAM are 0.29, 0.80, 1.60 dB for $N = 100000, 10000, 2000$, respectively. For 8-PAM, the gaps are 0.33, 0.84, 1.60 dB, respectively. The performance of D-IRA ring codes with different lengths shows that the optimized parameters under long-length codes also perform well on medium-length codes.

B. Examples of D-IRA Ring codes for Multi-user Networks

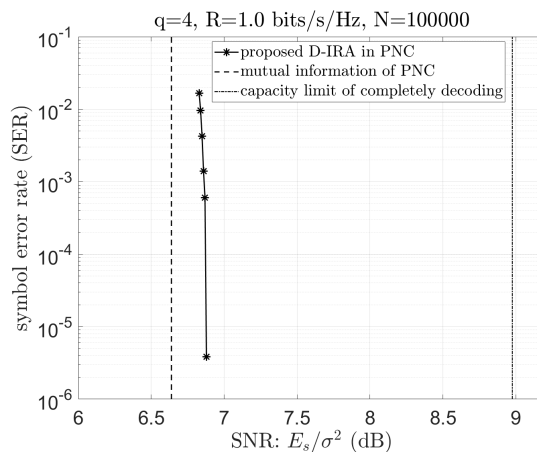


Fig. 11. Error-rate performance of the proposed D-IRA ring coded two-user CF with 4-PAM modulation.

1) *D-IRA ring coded CF*: Fig. 11 shows the error-rate performance of the proposed D-IRA ring coded CF scheme with two users, with 4-PAM signaling. For clarity of presentation, we first consider the simplest example of $h_1 = h_2 = 1$ and $\alpha_1 = \alpha_2 = 1$. It can be seen that at SER of 10^{-5} , the performance achieved by the proposed scheme is only 0.24 dB away from the CF mutual information [39]–[41]. The dashed line on the right side is the capacity limit w.r.t. completely decoding, obtained from the capacity region of two-user multiple-access channel [42]. The proposed D-IRA ring coded CF has an advantage of at least 2.34 dB. The performance advantage becomes greater for higher level of 2^m -PAM.

We further consider a system with a larger K over a Rayleigh fading channel. Fig. 12 shows the frame error rate (FER) of a linear PNC (CF) based MA scheme with the proposed D-IRA ring code of 4-PAM signaling. The number of users are $K = 8$ and there are $N_R = 4$ receive antennas, where the system load is 200%. The receiver is set compute $L = K = 8$ linear message combinations in parallel, where the symbol-wise APP calculation is extended to the multi-antenna. It is demonstrated that with D-IRA ring codes, structuring binning can be exploited in this overloaded MA setup. This leads to remarkable improvement over existing interleave-division MA (IDMA) and sparse-code MA (SCMA). Further improvement can be achieved by introducing successive computation, whose details can be found in [?].

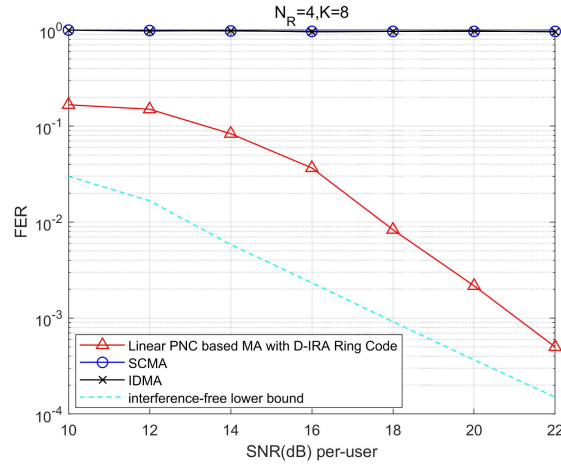


Fig. 12. FER of PNC (CF) based MA with proposed D-IRA ring code of 4-PAM signaling. The FERs of IDMA and SCMA do not decrease as SNR increases, as their iterative receivers fail to address the interference in this overloaded case. In contrast, the CF based MA scheme with D-IRA code performs within 3 dB the capacity limit. Further improvement can be achieved by introducing successive computation.

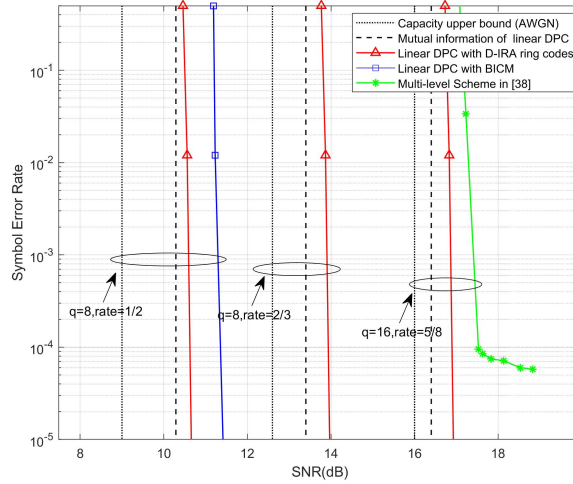


Fig. 13. Error rate performance of the proposed linear DPC with D-IRA ring codes.

2) *D-IRA ring coded DPC*: Fig. 13 plots the error rate performance of D-IRA ring coded DPC with $n=50000$. Our developed scheme exhibits gaps to the interference-free AWGN channel capacity upper bound by 1.36 and 0.91dB for rates 2 and 2.5 bits/symbol, respectively. We also include the performance of the BICM based DPC and multi-level based DPC scheme [35], where 4 levels are used with average coding rate of 5/8 per-level. The proposed scheme exhibits a 0.7 dB advantage at error rate of 10^{-4} . Similar observations are also observed for medium-length codes. Note that the implementation of the presented DPC is much simpler than the multi-level design in [35].

C. Complexity

Albeit the purpose of this work is not for complexity reduction, here we evaluate the complexity of the proposed scheme for comparison purpose. We consider the decoding complexity of the D-IRA ring

codes with FFT acceleration, whose details are given in Appendix. The belief propagation procedure in the iterative decoding constitutes the majority of complexity of the D-IRA codes, hence the complexity of the calculation of symbol-wise channel-intrinsic APPs in (6) is not evaluated. Following the convention, we only consider the complexity of the multiplication operations. Denote the length of the interleaver by Υ . There are totally $\Upsilon + 2n$ edges w.r.t. the CNs. For each edge, there are $2 \cdot 2^m \log_2(2^m)$ and $2^m \log_2(2^m)$ multiplications in FFT and IFFT separately. The calculated messages from FFT are multiplied, which require $4E[d_{c,i}^2]n2^m$ multiplications in total. The VNs require $E[d_{c,i}^2]n2^m$ multiplications.

Next consider BICM-ID with 2^m PAM. The number of outer-loop iterations for BICM-ID receiver is denoted by Ω . For fair comparison, consider that the degree distribution of the binary IRA code is identical to that of the 2^m D-IRA code. BICM requires $m\Omega$ binary decoding operations, where the order of complexity of each decoding is $O(2m)$. In contrast, a D-IRA ring code needs one 2^m -ary decoding, where the order of complexity is $O(2^m)$. For various m and Ω values, the complexity ratios between them are shown in Table. VII. The complexity of D-IRA ring codes is smaller than that of BICM with more than 4 outer-loop receiver iterations (up to 32-PAM). As the modulation level 2^m increases, the number of outer-loop iterations required to approach the near-capacity also increases in BICM-ID. Comparing to the $\text{GF}(2^m)$ IRA modulation codes, the D-IRA ring codes have exactly the same order of complexity.

TABLE VII
THE RATIOS BETWEEN THE COMPLEXITIES OF D-IRA RING CODES AND BICM.

	4-PAM	8-PAM	16-PAM	32-PAM
$\Omega=4$	25.0%	33.3%	50.0%	80.0%
$\Omega=6$	16.7%	22.2%	33.3%	53.3%
$\Omega=8$	12.5%	16.7%	25.0%	40.0%

D. Discussion of Ring Code Design for Medium and Short Packet Length

Previously, we showed that code profiles optimized for long codes are also competitive for medium-length-codes. A crucial subsequent future work along this research direction would be to investigate how to exploit the doubly-irregular structure in designing ring codes for scenarios with short packet length, e.g., the messages length k being 64, 128, \dots , 512. The design for such scenario will be based on optimization of the Euclidean distance spectrum of the 2^m -ary ring code with 2^m -PAM signaling, rather than the convergence behavior for long code presented in this paper. One possible way to address this task would be to use an ‘‘error pattern impulse’’ based method [43] to optimize the minimum distance of the ring code with doubly-irregular structure. Due to the nature of the 2^m -ary processing, the minimum girth is expected to be increased relative to conventional binary based coded modulation schemes, and

thus extremely low error-floor, e.g. frame error probability less than 10^{-7} is expected to be achieved. This future work is an interesting but quite challenging task, and is out of the scope of the current paper.

VII. CONCLUSIONS

This paper developed doubly irregular repeat accumulate (D-IRA) ring codes for 2^m -PAM signaling. The proposed practical ring codes feature the integer additive property of lattice codes. The irregular multipliers and irregular node degree distribution, and partial random interleavers, were designed to optimize the code profile. Numerical results demonstrated near-capacity in point-to-point channel without the need of outer-loop receiver iteration, as well as significant gains in multi-user networks with compute-forward and dirty paper coding. The proposed D-IRA ring codes provide a bridge between advanced notions in network information theory and practical multi-user networks. The development of D-IRA ring codes to realize other network information theory notions, such as Slepian-wolf coding, index coding, integer-forcing, etc., deserves further research efforts. The design of D-IRA ring codes of short code length requires the optimization of Euclidean distance spectrum, which is a challenging task to be studied in the future.

APPENDIX I FFT ACCELERATED CALCULATION FOR CHECK NODES

Let the vector $\mathbf{x} = (x_0, \dots, x_{q-1})$. We define the vector of its multiplication cycle as

$$\mathbf{x}^{\times g} \triangleq (x_0, x_g, x_{2\otimes g}, \dots, x_{(q-1)\otimes g}). \quad (46)$$

According to [26], [44], (8) can be rewritten with q -dimension DFT/IDFT transform for prime q :

$$\bar{\mathbf{l}} = \text{IDFT} \left(\prod_{n=1}^{d-1} \text{DFT}(\bar{\mathbf{r}}^n) \right), \quad (47)$$

where $\bar{\mathbf{r}}^n = (\mathbf{r}^n)^{\times h_n^{-1}}$ and the updated probability vector $\mathbf{l} = \bar{\mathbf{l}}^{\times (-h_d)}$.

For non-prime q , the superscript h_n^{-1} does not exist if h_n is a zero divisor. Reconsider expression (8) and treat one term on the left of equation $\sum_{n=1}^{d-1} h_n a_n = -h_d i$ as a whole, i.e. $h_s a_s = j$. Then we have

$$l_i = \sum_{\substack{a_1, \dots, a_{s-1}, a_{s+1}, \dots, a_{d-1} \in \mathbb{Z}_q, \\ \sum_{n=1, n \neq s}^{d-1} h_n a_n + j = -h_d i}} \left(\hat{r}_j^s \prod_{n=1, n \neq s}^{d-1} r_{a_n}^n \right), \quad (48)$$

where $\hat{r}_j^s = \sum_{a_s \in \mathbb{Z}_q, h_s \otimes a_s = j} r_{a_s}^s$. Therefore, a CN input-edge with probability vector \mathbf{r}^s and multiplier h_s is equivalent to having vector $\hat{\mathbf{r}}^s$ and multiplier 1. By equivalent substitution, there is $\bar{\mathbf{r}}^n = (\hat{\mathbf{r}}^n)^{\times 1^{-1}} = \hat{\mathbf{r}}^n$ in expression (47), which does not require the inverse of h_n . The expression is applicable to the case where some multipliers are zero-divisors, that is, the DFT accelerated calculation is also available for the

probability generation of D-IRA ring codes. For the case of $q = 2^m$, FFT and IFFT algorithms can also be used to replace the calculation of DFT and IDFT, which further reduces the amount of calculation.

REFERENCES

- [1] H. Jin, A. Khandekar, R. McEliece, *et al.*, “Irregular repeat-accumulate codes,” in *Proc. 2nd Int. Symp. Turbo codes and related topics*, pp. 1–8, Citeseer, 2000.
- [2] H. D. Pfister and I. Sason, “Accumulate-repeat-accumulate codes: Capacity-achieving ensembles of systematic codes for the erasure channel with bounded complexity,” *IEEE Trans. Inf. Theory*, vol. 53, no. 6, pp. 2088–2115, 2007.
- [3] A. Khandekar and R. Palanki, “Irregular repeat accumulate codes for non-binary modulation schemes,” in *Proceedings IEEE International Symposium on Information Theory*, p. 171, IEEE, 2002.
- [4] S. ten Brink and G. Kramer, “Design of repeat-accumulate codes for iterative detection and decoding,” *IEEE Trans. Signal Process.*, vol. 51, no. 11, pp. 2764–2772, 2003.
- [5] G. Caire, G. Taricco, and E. Biglieri, “Bit-interleaved coded modulation,” *IEEE Trans. Inf. Theory*, vol. 44, no. 3, pp. 927–946, 1998.
- [6] X. Li and J. A. Ritcey, “Trellis-coded modulation with bit interleaving and iterative decoding,” *IEEE Journal on Selected Areas in Communications*, vol. 17, no. 4, pp. 715–724, 1999.
- [7] S. Gadkari and K. Rose, “Time-division versus superposition coded modulation schemes for unequal error protection,” *IEEE Trans. Comm.*, vol. 47, no. 3, pp. 370–379, 1999.
- [8] X. Li, A. Chindapol, and J. Ritcey, “Bit-interleaved coded modulation with iterative decoding and 8 psk signaling,” *IEEE Trans. Comm.*, vol. 50, no. 8, pp. 1250–1257, 2002.
- [9] M.-C. Chiu, “Bandwidth-efficient modulation codes based on nonbinary irregular repeat–accumulate codes,” *IEEE Trans. Inf. Theory*, vol. 56, no. 1, pp. 152–167, 2009.
- [10] L. Yang, T. Yang, J. Yuan, and J. An, “Achieving the near-capacity of two-way relay channels with modulation-coded physical-layer network coding,” *IEEE Transactions on Wireless Communications*, vol. 14, no. 9, pp. 5225–5239, 2015.
- [11] S.-Y. Li, R. W. Yeung, and N. Cai, “Linear network coding,” *IEEE Trans. Inf. Theory*, vol. 49, no. 2, pp. 371–381, 2003.
- [12] R. Zamir, S. Shamai, and U. Erez, “Nested linear/lattice codes for structured multiterminal binning,” *IEEE Trans. Inf. Theory*, vol. 48, no. 6, pp. 1250–1276, 2002.
- [13] U. Erez and S. T. Brink, “A close-to-capacity dirty paper coding scheme,” *IEEE Trans. Inf. Theory*, vol. 51, no. 10, pp. 3417–3432, 2005.
- [14] B. Nazer and M. Gastpar, “Compute-and-forward: Harnessing interference through structured codes,” *IEEE Trans. Inf. Theory*, vol. 57, no. 10, pp. 6463–6486, 2011.
- [15] V. Cadambe and S. Jafar, “Interference alignment and the degrees of freedom of the K user interference channel,” *IEEE Trans. Inf. Theory*, vol. 54, no. 8, pp. 3425–3441, Aug. 2008.
- [16] V. Ntranos, V. Cadambe, B. Nazer, and G. Caire, “Integer-forcing interference alignment,” *IEEE ISIT*, pp. 574–578, 2013.
- [17] T. Yang, “Distributed MIMO broadcasting: Reverse compute-and-forward and signal-space alignment,” *IEEE Trans. Wireless Comm.*, vol. 16, no. 1, pp. 581–593, 2017.
- [18] G. Byers and F. Takawira, “EXIT charts for non-binary ldpc codes,” in *IEEE International Conference on Communications, 2005. ICC 2005. 2005*, vol. 1, pp. 652–657 Vol. 1, 2005.
- [19] J. Zhu and M. Gastpar, “Gaussian multiple access via compute-and-forward,” *IEEE Trans. Inf. Theory*, vol. 63, no. 5, pp. 2678–2695, 2017.
- [20] T. Yang, L. Yang, Y. J. Guo, and J. Yuan, “A non-orthogonal multiple-access scheme using reliable physical-layer network coding and cascade-computation decoding,” *IEEE Trans. Wireless Comm.*, vol. 16, no. 3, pp. 1633–1645, 2017.

- [21] T. Yang and I. B. Collings, "On the optimal design and performance of linear physical-layer network coding for fading two-way relay channels," *IEEE Trans. Wireless Comm.*, vol. 13, no. 2, pp. 956–967, Feb. 2014.
- [22] G. Forney, "Coset codes. ii. binary lattices and related codes," *IEEE Trans. Inf. Theory*, vol. 34, no. 5, pp. 1152–1187, 1988.
- [23] N. Sommer, M. Feder, and O. Shalvi, "Low-density lattice codes," *IEEE Trans. Inf. Theory*, vol. 54, no. 4, pp. 1561–1585, 2008.
- [24] S. Lin and D. J. Costello, "Error control coding," *Prentice Hall*, 2004.
- [25] S. Ten Brink, "Convergence behavior of iteratively decoded parallel concatenated codes," *IEEE Trans. Comm.*, vol. 49, no. 10, pp. 1727–1737, 2001.
- [26] A. Bannatan and D. Burshtein, "Design and analysis of nonbinary LDPC codes for arbitrary discrete-memoryless channels," *IEEE Trans. Inf. Theory*, vol. 52, no. 2, pp. 549–583, 2006.
- [27] S. Sawyer, "Generalized inverses: how to invert a non-invertible matrix," 2006.
- [28] S. Ten Brink, G. Kramer, and A. Ashikhmin, "Design of low-density parity-check codes for modulation and detection," *IEEE Trans. Comm.*, vol. 52, no. 4, pp. 670–678, 2004.
- [29] T. Richardson and R. Urbanke, "The capacity of low-density parity-check codes under message-passing decoding," *IEEE Trans. Inf. Theory*, vol. 47, no. 2, pp. 599–618, 2001.
- [30] T. Richardson, M. Shokrollahi, and R. Urbanke, "Design of capacity-approaching irregular low-density parity-check codes," *IEEE Trans. Inf. Theory*, vol. 47, no. 2, pp. 619–637, 2001.
- [31] J. Hou, P. Siegel, L. Milstein, and H. Pfister, "Capacity-approaching bandwidth-efficient coded modulation schemes based on low-density parity-check codes," *IEEE Trans. Inf. Theory*, vol. 49, no. 9, pp. 2141–2155, 2003.
- [32] C.-C. Wang, S. Kulkarni, and H. Poor, "Density evolution for asymmetric memoryless channels," *IEEE Trans. Inf. Theory*, vol. 51, no. 12, pp. 4216–4236, 2005.
- [33] S.-Y. Chung, T. Richardson, and R. Urbanke, "Analysis of sum-product decoding of low-density parity-check codes using a gaussian approximation," *IEEE Trans. Inf. Theory*, vol. 47, no. 2, pp. 657–670, 2001.
- [34] H. Pfister and P. Siegel, "The serial concatenation of rate-1 codes through uniform random interleavers," *IEEE Trans. Inf. Theory*, vol. 49, no. 6, pp. 1425–1438, 2003.
- [35] M. Uppal, G. Yue, Y. Xin, X. Wang, and Z. Xiong, "A robust multi-level design for dirty-paper coding," *IEEE Trans. Comm.*, vol. 61, no. 7, pp. 2612–2623, 2013.
- [36] J. Zhan, B. Nazer, U. Erez, and M. Gastpar, "Integer-forcing linear receivers," *IEEE Trans. Inf. Theory*, vol. 60, no. 12, pp. 7661–7685, Dec. 2014.
- [37] M. Costa, "Writing on dirty paper (corresp.)," *IEEE Trans. Inf. Theory*, vol. 29, no. 3, pp. 439–441, 1983.
- [38] T. Yang, "A simple approach to practical dirty paper coding," *Accepted to IEEE ICC 2022*, 2022.
- [39] B. Nazer and M. Gastpar, "Computation over multiple-access channels," *IEEE Trans. Inf. Theory*, vol. 53, no. 10, pp. 3498–3516, 2007.
- [40] S. H. Lim, C. Feng, A. Pastore, B. Nazer, and M. Gastpar, "A joint typicality approach to compute-forward," *IEEE Trans. Inf. Theory*, vol. 64, no. 12, pp. 7657–7685, 2018.
- [41] M. Qiu, L. Yang, Y. Xie, and J. Yuan, "On the design of multi-dimensional irregular repeat-accumulate lattice codes," *IEEE Transactions on Communications*, vol. 66, no. 2, pp. 478–492, 2018.
- [42] D. Tse and P. Viswanath, *Fundamentals of wireless communication*. Cambridge university press, 2005.
- [43] L. Liu, J. Huang, W. Zhou, and S. Zhou, "Computing the minimum distance of nonbinary ldpc codes," *IEEE Trans. on Comm.*, vol. 60, no. 7, pp. 1753–1758, 2012.
- [44] A. Goupil, M. Colas, G. Gelle, and D. Declercq, "FFT-based BP decoding of general LDPC codes over abelian groups," *IEEE Trans. Comm.*, vol. 55, no. 4, pp. 644–649, 2007.